Antiferromagnetic order in $Li(Ni_{1-x}Fe_x)PO_4$ ($x = 0.06, 0.20$)

Anne S. Zimmermann,[1] Elke Sondermann,[1] Jiying Li,[2] David Vaknin,[2] and Manfred Fiebig[3,*]
[1]*Helmholtz-Institut für Strahlen- und Kernphysik, Universität Bonn, Nussallee 14-16, 53115 Bonn, Germany*
[2]*Ames Laboratory and Department of Physics and Astronomy, Iowa State University, Ames, Iowa 50011, USA*
[3]*Department of Materials, ETH Zurich, Wolfgang-Pauli-Strasse 10, 8093 Zurich, Switzerland*
(Received 8 April 2013; published 19 July 2013)

The investigation of $Li(Ni_{1-x}Fe_x)PO_4$ by optical second harmonic generation yields the competition of the antiferromagnetic (AFM) structures and 180° domain patterns found in the end compounds $LiNiPO_4$ (point group $mm'm$, spins along z) and $LiFePO_4$ (point group mmm', spins along y). While the AFM order and the distribution of the AFM domains of $LiNiPO_4$ are unaffected by the ion substitution at $x = 0.06$, striking changes are observed at $x = 0.20$. Fe^{2+} is dominant in establishing the magnetic order. For $x = 0.20$ the magnetic order of the solid solution interpolates the magnetic order of its end compounds by exhibiting an orientation of the spins in the (100) plane which include an angle of $40° \pm 3°$ with respect to the y axis toward 0 K (point group m). The associated AFM domains form rods of a few millimeters length and ~10 μm width occurring in neither of the end compounds. Mechanisms responsible for the magnetic order and domain pattern (180° domains still being one of the least explored aspects of AFM materials in spite of their omnipresence) are discussed.

DOI: 10.1103/PhysRevB.88.014420 PACS number(s): 75.50.Ee, 75.60.Ch, 75.30.Gw, 42.65.Ky

I. INTRODUCTION: 180° ANTIFERROMAGNETISM IN THE $LiMPO_4$ SYSTEM

The significance of antiferromagnetism for practical applications has continuously been increasing during the past years. Antiferromagnetic (AFM) order is predominant in strongly correlated systems like colossal-magnetoresistance compounds[1] or as a precursor to high-temperature superconductors.[2] AFM nanostructures have even been shown to exhibit the type of bistable switching that is fundamental for data storage applications.[3] Due to the absence of a net magnetization, AFM compounds were furthermore proposed as candidates for rapid spin manipulation as no angular momentum has to be conserved.[4–6] Yet, the main interest in AFM compounds originates from the directional coupling between the spins in an antiferromagnet and those in an adjacent ferromagnet, an effect termed exchange bias.[7] The exchange-bias effect is a key to advanced magnetic devices such as magnetic read heads[8,9] and magnetic memory cells.[10]

To a large extent the characteristics of the aforementioned phenomena are defined by the respective distribution of the AFM domains. As the energy change under applied magnetic field is close to zero in AFM compounds the distribution of domains is determined by subtle, little understood criteria like gradient fields in domain walls, magnetostriction, magnetic anisotropy, and defects. Among the different types of AFM domain states the 180° domain states are most subtle because opposite 180° domains (also termed spin-reversal or antiphase domains) differ in the reversal of all their respective spins only. The walls between 180° domains are not subject to strain or other mechanical or electrostatic effects so that the investigation of compounds with just a pair of 180° domain states leads to magnetic interactions relevant for the distribution of AFM domains that are otherwise obscured by stronger effects. In spite of their omnipresence, the distribution of 180° domain states is one of the least explored aspects of antiferromagnetism which is mostly due to the experimental difficulties to access them.

An ideal system for probing such a domain structure is given by the lithium orthophosphates ($LiMPO_4$ with M = Mn, Fe, Co, Ni). All four compounds are crystallographically isostructural; only their AFM order differs in the axis along which the spins are oriented. Thus, the system offers the opportunity to study fundamental mechanisms of 180°-type AFM order in a range of similar, yet not identical compounds. The structure of the $LiMPO_4$ compounds has been studied since the early 1960s.[11–13] They are insulators which, crystallographically, belong to the orthorhombic olivine family.[14] The orthorhombic cell contains four formula units and belongs to the space group $Pnma$ (No. 62, D_{2h}^{16}).[15–17] Below the Néel temperature T_N, which ranges between 20.8 and 50 K,[12,13,18] long-range AFM order emerges in all four compounds. Originally, neutron diffraction revealed the same type of compensated spin arrangement for all four compounds with differences in the spin direction only[19]: along x for Mn^{2+}, along y for Co^{2+} and Fe^{2+}, and along z for Ni^{2+}.[12,13,18] More recent neutron diffraction data revealed incommensurate phases[20] or a small canting of the spins away from the principal axes for some of the compounds.[21–23] The latter indicates a lower magnetic symmetry than originally proposed. The lower symmetry permits a variety of unusual effects, such as a weak magnetic moment *along* the spin direction,[24–26] a complex temperature dependence of the linear magnetoelectric effect,[27,28] or ferrotoroidicity as a novel type of ferroic order.[29,30] A detailed discussion of the mechanisms determining the magnetic structure and their relation to the results presented here will follow in Sec. III C.

Despite their similar crystallographic and magnetic structure, drastic differences in the domain topography were observed in the $LiMPO_4$ compounds.[31–33] The three-dimensional distribution of the domains in $LiCoPO_4$ and $LiFePO_4$ was found to be isotropic, thus contrasting the pronounced quasi-two-dimensional magnetic nature of the compound. Even in the case of $LiNiPO_4$, where an anisotropic domain structure is found, this anisotropy does not correspond to the magnetic and crystallographic anisotropy of the compound.

 ©2013 American Physical Society

The first step in resolving the mechanisms leading to the different manifestation of the AFM 180° domains is to investigate the interplay of the competing phases. For this purpose we extended our investigation beyond that of the two end members to $LiMPO_4$ samples composed of two constituents M. In this report we analyze the magnetic phases and the corresponding bulk domain distribution in $Li(Ni_{1-x}Fe_x)PO_4$ with $x = 0.06, 0.20$ with optical second harmonic generation (SHG) coupling linearly to the AFM order parameter. We find a pronounced dominance of the Fe^{2+} over the Ni^{2+} ions in establishing the magnetic order. Whereas the magnetic order of the Fe-substituted samples interpolates the magnetic order of its end compounds, the AFM domain structure reveals fundamental differences with respect to those in $LiNiPO_4$ and $LiFePO_4$. The underlying mechanisms are discussed.

The $Li(Ni_{1-x}Fe_x)PO_4$ samples were grown by the standard flux-growth method at the Ames Laboratory at Iowa State University. The composition of the crystals was confirmed by a chemical analysis, and x-ray diffraction measurements that corroborated the $LiMPO_4$-like crystallographic structure and symmetry of the Fe-substituted samples.[34] Magnetic susceptibility and neutron-diffraction measurements favored a low-temperature ground state of the Fe-substituted samples that is AFM with a magnetic arrangement similar to that found in pure $LiNiPO_4$.[34] Furthermore, it was found that the incommensurate phase of $LiNiPO_4$[20] is continuously weakened with increasing x and absent at $x = 0.20$ where the transition to the AFM phase has become second order.[34]

II. EXPERIMENT

Experimental techniques for imaging AFM domain structures are rare. The topography of AFM 180° domains is particularly difficult to analyze by diffraction techniques because polarized neutrons are required for their observation while magnetostriction and linear x-ray dichroism do not distinguish between the opposite domain states.[35] A very convenient way for imaging AFM domains, particularly 180° domains, is optical SHG. An electromagnetic light field $\vec{E}$ at frequency ω is incident onto a crystal and induces a polarization $\vec{P}$ at frequency 2ω, which acts as source of an emitted, frequency-doubled light wave. This is expressed by

$$\vec{P}_i(2\omega) = \epsilon_0 \chi_{ijk} \vec{E}_j(\omega) \vec{E}_k(\omega), \quad (1)$$

with $\hat{\chi}$ as SHG susceptibility. The tensor $\hat{\chi}$ can include contributions that couple linearly to the AFM order parameter and are therefore present below T_N only. In addition, SHG can distinguish between 180° domain states with opposite orientation of the AFM order parameter through a change of sign of $\vec{P}(2\omega)$. The sign change corresponds to a 180° phase difference between the corresponding SHG light waves and can be converted into an intensity difference in a SHG interference experiment. This has been used to investigate the spatial distribution of AFM 180° domains in a variety of oxide compounds.[36] Access to the magnetic and crystallographic structure by SHG is governed by the Neumann principle according to which any symmetry operation applied to a system leaves its physical properties invariant. This determines the set of nonzero and independent tensor components χ_{ijk} in Eq. (1).[37] In turn, experimental determination of these tensor components reveals the crystallographic and magnetic symmetry and structure of a compound. SHG in the electric-dipole approximation of Eq. (1) is only allowed in noncentrosymmetric compounds. In the case of the $LiMPO_4$ system the AFM spin arrangement breaks the inversion symmetry of the otherwise centrosymmetric crystallographic lattice so that SHG provides a background-free probe of the magnetic order. In the following symmetry analysis and in Table I we therefore restrict ourselves to the discussion of electric-dipole contributions of the electromagnetic light fields to the SHG process, whereas the generally much weaker higher-order multipole contributions are omitted.

TABLE I. Experimentally observed SHG tensor components, magnetic point symmetry, and spin direction in $LiNiPO_4$, $LiFePO_4$, and $Li(Ni_{0.80}Fe_{0.20})PO_4$. Because of the breaking of inversion symmetry by the magnetic order, SHG contributions are restricted to the electric-dipole approximation of the involved light fields according to Eq. (1), whereas the generally much weaker higher-order multipole contributions are omitted.

Compound	Tensor components	Point group	Spin
$LiFePO_4$	$\chi^{Fe}_{xxz}, \chi^{Fe}_{zxx}, \chi^{Fe}_{zyy}, \chi^{Fe}_{yyz}, \chi^{Fe}_{zzz}$	mmm'	y
$LiNiPO_4$	$\chi^{Ni}_{yxx}, \chi^{Ni}_{xxy}, \chi^{Ni}_{yzz}, \chi^{Ni}_{yyy}, \chi^{Ni}_{zzy}$	$mm'm$	z
$Li(Ni_{0.80}Fe_{0.20})PO_4$	$\chi^{Fe}_{zzz}, \chi^{Fe}_{zyy}, \chi^{Fe}_{yyz}, \chi^{Fe}_{zxx}, \chi^{Ni}_{yxx}$	m_x	(y,z)

In the experiment, sets of three $Li(Ni_{0.94}Fe_{0.06})PO_4$ and three $Li(Ni_{0.80}Fe_{0.20})PO_4$ bulk single crystals with lateral dimensions of 1–3 mm and a thickness of 10–300 μm were used. The three platelets of a set were cut along the (100), (010), and (001) plane, respectively, and polished with an aqueous colloidal silica slurry. Several such sets were prepared in order to verify the reproducibility of the results among different samples. A transmission setup was employed in which the samples were mounted in a liquid-helium cooled variable-temperature cryostat and excited with light pulses of 3 ns and ~1 mJ emitted from an optical parametric oscillator. The polarization of the incident light was set with a half-wave plate. Behind the cryostat, the SHG light was analyzed with a polarization filter while the fundamental light was suppressed by color filters. The SHG light was projected onto a liquid-nitrogen cooled digital camera by a telephoto lens.[36]

Because of optical absorption the illumination of the samples with the laser beam lead to heating on the order of a few Kelvin. Temperature values in this report have been corrected by this effect. The correction value was determined by measuring the transition temperature T_N for various laser intensities. This allows us to extrapolate the real value of T_N and, thus, the laser-induced temperature shift. In the case of Fig. 1(c), T_N was furthermore verified with an alternative laser system emitting pulses of 130 fs.

III. RESULTS AND DISCUSSION

A. SHG spectroscopy

1. $Li(Ni_{0.94}Fe_{0.06})PO_4$

Figures 1(a) and 1(b) shows the SHG spectra of $Li(Ni_{0.94}Fe_{0.06})PO_4$ taken at 10 K with $2\hbar\omega$ ranging from 1.8 to

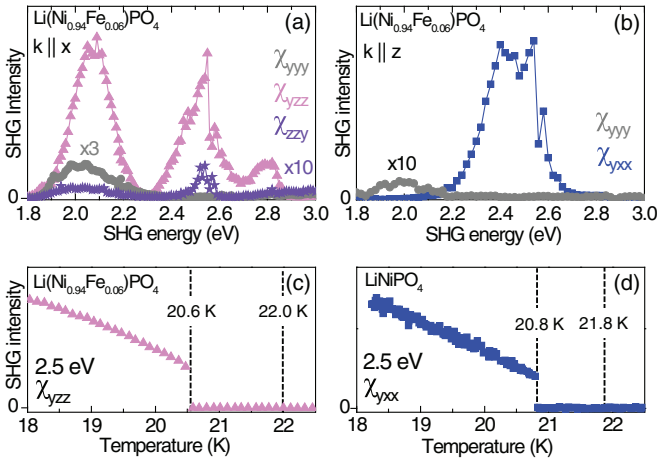

FIG. 1. (Color online) (a) and (b) Spectral and (c) temperature dependence of SHG in $Li(Ni_{0.97}Fe_{0.03})PO_4$. (d) Temperature dependence of SHG in $LiNiPO_4$ shown for comparison. The SHG energy refers to the value of $2\hbar\omega$ with ω as frequency of the incident fundamental light.

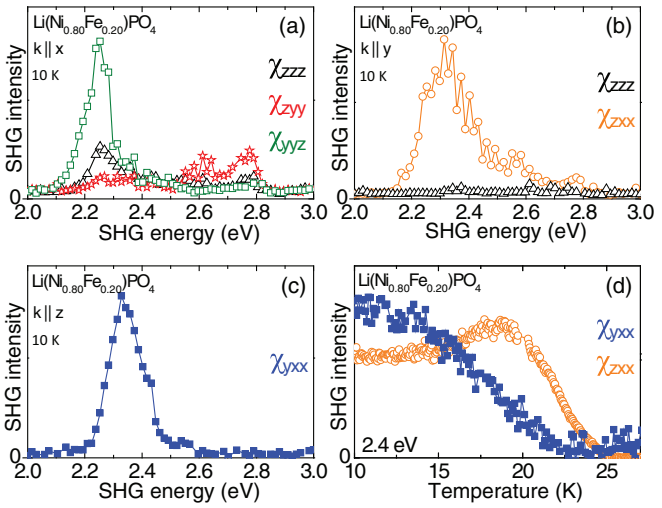

FIG. 2. (Color online) Spectral and temperature dependence of various SHG contributions in $Li(Ni_{0.80}Fe_{0.20})PO_4$.

3.0 eV. Nonzero contributions to SHG in $Li(Ni_{0.94}Fe_{0.06})PO_4$ are obtained from $\chi_{yyy}, \chi_{yzz}, \chi_{zzy}, \chi_{yxx}$. This points uniquely to the magnetic point symmetry $mm'm$ with spins aligned along the z axis.[37] Thus, SHG data, just like neutron diffraction data, reveal that the low-temperature ground state of $Li(Ni_{0.94}Fe_{0.06})PO_4$ is AFM with a magnetic arrangement similar to that found in pure $LiNiPO_4$.[31,34]

The magnetic origin of the SHG contributions is confirmed by temperature-dependent measurements. In Fig. 1(c) the temperature dependence of the SHG contribution from χ_{yzz} measured at 2.5 eV in the temperature range 18–22.5 K is shown. The SHG intensity decreases steadily with increasing temperature. The slope is approximately linear until the SHG signal disappears abruptly at 20.6 K. An extrapolation of the linear dependence leads to a zero crossing at 22.0 K.

A similar behavior was observed in $LiNiPO_4$ where the abrupt drop of the SHG intensity was associated with the transition from the commensurate to the incommensurate phase[31,32] [see Fig. 1(d)]. Apparently the same intermediate incommensurate phase, with only little modification of the critical temperatures, is present in $Li(Ni_{0.94}Fe_{0.06})PO_4$.

2. $Li(Ni_{0.80}Fe_{0.20})PO_4$

Figures 2(a) to 2(c) display the SHG spectra of $Li(Ni_{0.80}Fe_{0.20})PO_4$ obtained at 10 K with $2\hbar\omega$ in the range 2.0–3.0 eV. As for $Li(Ni_{0.94}Fe_{0.06})PO_4$ rich spectra with a pronounced polarization dependence are found. As summarized in Table I, SHG contributions are obtained from χ_{zzz}, χ_{zyy}, χ_{yyz}, χ_{zxx}, χ_{yxx}. Strikingly, except from χ_{yxx} none of these components coincide with the ones expected for a magnetic point group $mm'm$, i.e., as in $LiNiPO_4$ with spins along the z axis. This was the spin structure favored for $Li(Ni_{0.80}Fe_{0.20})PO_4$ thus far.[34] Instead, the additional four components χ_{zxx}, χ_{zyy}, χ_{yyz}, and χ_{zzz} coincide with tensor components allowed and experimentally observed for $LiFePO_4$ with the magnetic point group mmm' and spins aligned along the y axis.[32]

A straightforward explanation for the presence of the observed tensor components that we propose is a canted spin arrangement with spins pointing in a direction in between the y and the z axis. The magnetic point group compatible with such a canted spin arrangement is m. It permits all the SHG tensor components of the point groups $mm'm$ ($\sim LiNiPO_4$) and mmm' ($\sim LiFePO_4$) to be nonzero.[37] These components are summarized in Table I. Note that in addition to the observed components, contributions from five more SHG susceptibilities are also symmetry allowed. Their absence in our data is most likely caused by the specific transmission and absorption properties of $Li(Ni_{0.80}Fe_{0.20})PO_4$ at ω and 2ω.

In Fig. 3(a) an exemplary sketch of such a canted spin is depicted along with its projection of the spin onto the y and z axis. In addition, the largest tensor component that is sensitive to the respective spin direction is given. In total, χ_{zxx}, χ_{zyy}, χ_{yyz}, and χ_{zzz} are assigned to the spin contribution parallel to the y axis, while χ_{yxx} is attributed to the spin contribution along the z axis.

In order to verify the magnetic origin of the SHG signals and determine the order and temperature of the phase transition, the temperature dependence of the SHG signal from the two susceptibilities pointed out in Fig. 3(a) is depicted in Fig. 2(d). The two SHG contributions exhibit a strikingly different behavior. The SHG signal from χ_{zxx} remains constant up to 15 K. Between 15 to 18 K the SHG signal increases gradually by 20%, followed by a rapid decrease above 18 K until it reaches zero at $T_2 = 25.0$ K. In contrast the SHG signal from

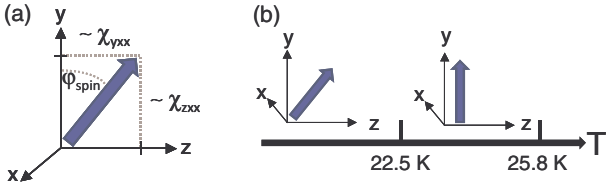

FIG. 3. (Color online) (a) Relation between spin components and SHG susceptibilities in the (100) plane of $Li(Ni_{0.80}Fe_{0.20})PO_4$. (b) Sketch of the temperature dependent spin orientation.

χ_{yxx} steadily decreases with increasing temperature until it vanishes at $T_1 = 22.5$ K.

The different temperature dependence of the two tensor components can be explained by taking into account the orientation of the spins in the (100) plane and its change with temperature as sketched in Fig. 3(b). With increasing temperature the spins rotate toward the y axis. This is expressed by the *decrease* of the SHG signal from χ_{yxx} while a simultaneous *increase* of the SHG signal from χ_{zxx} occurs. The disappearance of the SHG signal at $T_1 = 22.5$ K indicates the drop of the spin-rotation angle to zero, i.e., above T_1 the spins point straight along the y axis. After passing a maximum at 18 K SHG from χ_{zxx} begins to drop because of the characteristic decrease of the order parameter toward the paramagnetic state which is entered when the net SHG intensity drops to zero at $T_N = T_2 = 25.0$ K. The temperature dependence of all SHG contributions is continuous up to T_N which points to second-order phase transitions in $Li(Ni_{0.80}Fe_{0.20})PO_4$ without any intermediate incommensurate phase.

The rotation angle φ_{spin}, here defined as the angle between the spin direction and the y axis [see Fig. 3(a)], can be derived from the temperature dependence of the SHG signal $I_{SHG} \propto |\chi_{zxx}|^2$ as a geometric projection effect.[38,39] As Fig. 3(a) shows, the rotation of the magnetic moment reduces its y component, and with it χ_{zxx}, according to a cosine relation. In terms of SHG intensities this is expressed as

$$\varphi_{spin} = \arccos \sqrt{\frac{I_{SHG}(\varphi_{spin}, T)}{I_{SHG}(0, T)}}. \quad (2)$$

Here $I_{SHG}(\varphi_{spin}, T)$ is the measured SHG intensity from χ_{zxx} and $I_{SHG}(0, T)$ is the SHG intensity that would be obtained in the absence of spin rotation. In order to find the latter value, a phenomenological relation of the type $I_{SHG}(0, T) = I_{SHG}(0, 0) \cdot (1 - T/T_N)^C$ is fitted to the temperature-dependent SHG contribution from χ_{zxx} in the range between 22.5 and 25.0 K, where the spins are aligned along the y axis, followed by an extrapolation of the fitted relation down to 5 K [see Fig. 4(a)]. Figure 4(b) shows the temperature dependence of the spin angle thus derived from Eq. (2). We find a value $\varphi_{spin} = 40^\circ \pm 3^\circ$ that remains stable up to about 15 K and is followed by a continuous decrease down to $\varphi_{spin} = 0^\circ$ at T_1.

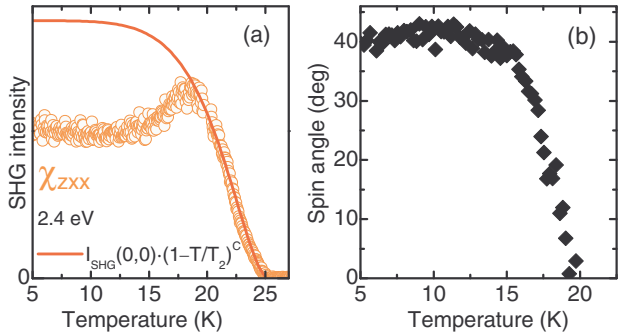

FIG. 4. (Color online) Temperature dependence of the spin angle quantifying the spin rotation in the (100) plane of $Li(Ni_{0.80}Fe_{0.20})PO_4$. (a) Data points: Temperature dependence of the SHG intensity from χ_{zxx} at 2.40 eV. Red line: Fit of the relation $I_{SHG}(0, T) = I_{SHG}(0, 0) \cdot (1 - T/T_N)^C$ to the temperature dependence of the SHG intensity in (a). The fit was applied in the range 20–25 K and extrapolated toward 0 K. (b) Temperature dependence of the spin angle derived from the difference between the data points and the extrapolated fit for a spin angle of zero in (a). Above 20 K the values of $\cos \varphi_{spin}$ vary around 1 and are thus not shown.

B. Domain topography

As mentioned, $LiNiPO_4$ and $LiFePO_4$ reveal very different distributions of their AFM domains: a highly anisotropic one in the former and an isotropic one in the latter compound.[37] Therefore the observation of the AFM domains in $Li(Ni_{1-x}Fe_x)PO_4$ with its competing spin orientations is of particular interest. Figure 5 shows the distribution of the AFM 180° domains on the (100), (010), and (001) faces of the $Li(Ni_{0.94}Fe_{0.06})PO_4$ and $Li(Ni_{0.80}Fe_{0.20})PO_4$ samples at 10 K. The (100) and (001) faces of $Li(Ni_{0.94}Fe_{0.06})PO_4$ reveal tightly spaced dark nonintersecting lines extending parallel to the crystallographic z or x axis, respectively. The lines correspond to the walls separating opposite 180° domains. Because of the aforementioned 180° phase shift between the SHG light

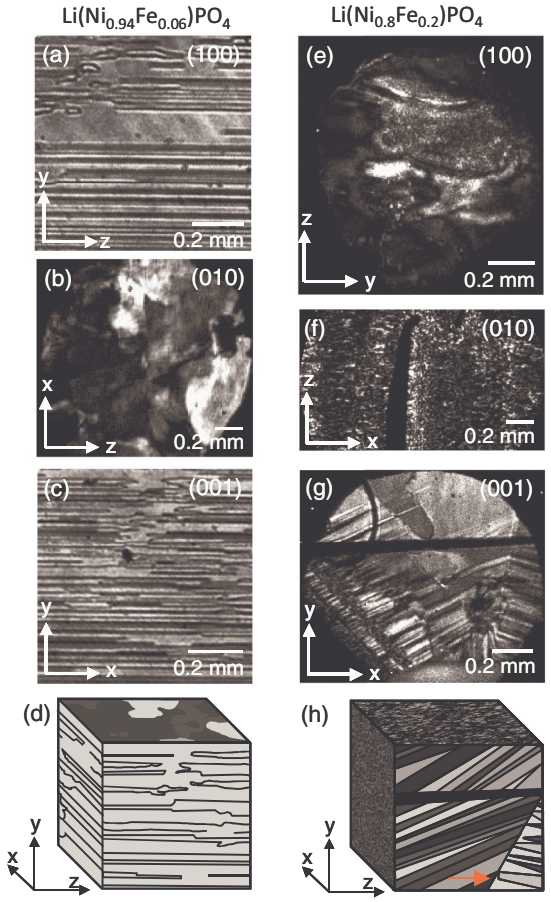

FIG. 5. (Color online) (a–c) and (e–g) Images of the AFM domain structure in $Li(Ni_{0.94}Fe_{0.06})PO_4$ and $Li(Ni_{0.80}Fe_{0.20})PO_4$ at 10 K and (d) and (h) three-dimensional sketches of the domain structures as observed by SHG. The broad vertical and horizontal dark stripe in images (f) and (g), respectively, is caused by an internal crack. The red arrow in the sketch in (h) indicates a sample-specific pinning line at which a change of slope of the domain walls is observed after each heating cycle through T_N.

waves emitted from opposite domains destructive interference at the walls leads to local cancellation.[40] On the (010) face a network of curved intersecting lines separating isotropic regions of different brightness with lateral dimensions on the order of 0.1 mm is observed. These patterns are caused by platelets of AFM 180° domains extended in the xz plane and stacked along the y axis. Perpendicular to the (010) face the domains are so thin that light from two or more of the stacked domains interferes, thus producing differently shaded regions and pseudointersections of domain walls. The domain pattern observed in Figs. 5(a) to 5(c) changes with every heating cycle through T_N but the qualitative structure remains unchanged in all samples.

In total, $Li(Ni_{0.94}Fe_{0.06})PO_4$ reveals an anisotropic distribution of domains which does not correspond to the magnetic anisotropy of the compound: The quasi-two-dimensional magnetic order occurs with respect to the yz plane, whereas the domain platelets are formed in the xz plane. A combination of the SHG images obtained on the different faces of the sample leads to a three-dimensional distribution as sketched in Fig. 5(d). We see that the domain structure of $Li(Ni_{0.94}Fe_{0.06})PO_4$ fully resembles that already observed in many $LiNiPO_4$ samples,[31] i.e., the Fe substitution of 6% has no detectable influence on the shape and distribution of the AFM domains.

In contrast, the domain structure observed on $Li(Ni_{0.80}Fe_{0.20})PO_4$ does not resemble either one of its end compounds. The (001) face yields stripes varying substantially in length, width, orientation, and brightness. As before, the variation in brightness is associated with the interference of SHG from domains stacked perpendicular to the surface. However, instead of the xz platelets found in $LiNiPO_4$ we now have rod-shaped domains within the xy plane with straight walls pointing in directions that coincide neither with the x nor the y axis. From the (100)- and (010)-oriented sides these assemblies of rods lead to a grainy distribution of the SHG intensity. This is caused by the distribution of domain walls that are so closely spaced that they are not spatially separable anymore within the optical resolution of about 10 μm of the experiment. This arrangement is summarized in the three-dimensional sketch in Fig. 5(h). Qualitatively the domain structure is found in all the $Li(Ni_{0.80}Fe_{0.20})PO_4$ samples investigated by us even though the explicit distribution of domains changes with each heating cycle through T_N. Minor sample-specific pinning effects are present. For example, the line at which a change of slope of the domain walls occurs as indicated by the red arrow in Fig. 5(h) is present after each heating cycle. It may be argued that the (100) and (010) faces were imaged with SHG light coupling to the z component of the spins, whereas the (001) face shows the domain pattern for the y component of the spins. However, here we found that the orientation of the spins along the y and the z axis is coupled: Both components lead to the same domain structure shown in Figs. 6(a) and 6(b).

Figures 6(c) and 6(d) repeat the exposures of Figs. 6(a) and 6(b) after heating the sample to a temperature between T_1 and T_2. Figure 6(c) is now dark because it refers to the z component of the spins which is zero in this temperature range. Figure 6(d) reveals a homogeneous distribution of the SHG intensity which shows that along with the orientation

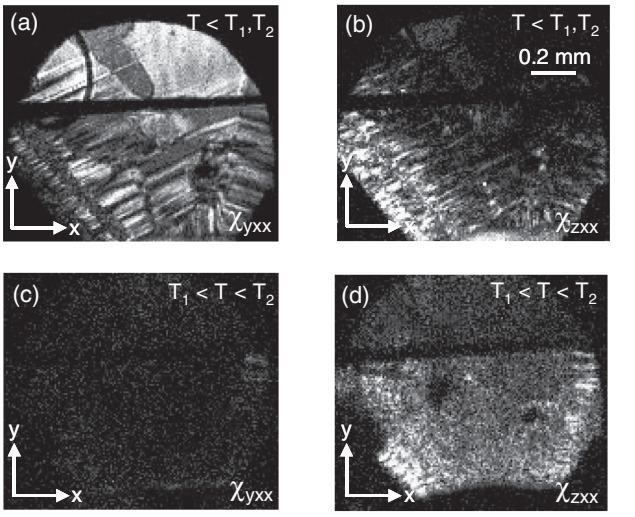

FIG. 6. Comparison of the domain structures associated with the y and z component of the spins in $LiNi_{0.80}Fe_{0.20}PO_4$. (a) and (c) Image taken on the (001) face with SHG from χ_{yxx} coupling to the y component. SHG energy is 2.35 eV. (b) and (d) Image taken on the (001) face with SHG from χ_{zxx} coupling to the z component. SHG energy is 2.35 eV. The dark horizontal region in the upper part of the sample is caused by an internal crack.

of the spins along the y axis the sample has dropped into a single-domain state. Although the spins are now ordered identical to $LiFePO_4$ the corresponding domain structure is nevertheless strikingly different.

C. Discussion of the magnetic structure

As mentioned, AFM 180° domain structures are one of the least explored aspects of AFM order. This shortcoming, due to the experimental difficulties to observe them, sharply contrasts their relevance—AFM 180° domain states occur in *any* type of AFM order. Since there is no comprehensive theory yet describing the distribution of AFM 180° domains we will restrict ourselves to a cautious discussion of mechanisms that determine the magnetic order and domain structures revealed in Figs. 1 to 6.

For the investigation of the magnetic order in the $LiMPO_4$ family up to five magnetic exchange paths are taken into account. The system is described as Ising-like between two and three dimensions and composed of antiferromagnetically ordered corrugated yz planes weakly coupled along the x axis.[23] Within the yz planes nearest-neighbor (NN) M–O–M superexchange competes with higher-order NNN exchange via M–O–O–M or even M–O–P–O–M paths.[41] Although the NN superexchange is strongest, the NNN interactions cannot be neglected and promote frustration.[34] The NN interplane coupling along a is of the M–O–P–O–M type and about one order of magnitude weaker than the in-plane exchange. In the leading order, the interplane exchange is frustrated but this frustration is resolved by higher-order coupling effects which are also suspected to be responsible for a small spin canting away from the principal axes and the "weak ferrimagnetism" observed in the $LiMPO_4$ series.[22]

Differences between the magnetic structure of the four $LiMPO_4$ compounds are small. First, in spite of the identical type of AFM spin arrangement, the *direction* of the magnetic moments differs (Mn $\sim x$, Fe/Co $\sim y$, Ni $\sim z$).[12,13,18] All structural analyses relate this to the single-ion anisotropy. A model quantifying the actual spin direction for the different $LiMPO_4$ compounds is still under development.[42] It can already be said that an important contribution to the single-ion anisotropy is the spin-orbit interaction. Since the change of the orbital filling is one of the most characteristic aspects of the $LiMPO_4$ series, it is reasonable to assume that this comes along with changes in the single-ion anisotropy.

Here our data indicate that the Fe^{2+} ions are associated with an unusually large single-ion anisotropy. A replacement of only 20% of the Ni^{2+} ions is sufficient to reset the easy-axis direction. This is in agreement with experiments on $LiMnPO_4$ where a Fe substitution of 30% (or less) achieves this purpose.[43] Furthermore, the Fe substitution readily suppresses the incommensurate magnetic phase of $LiNiPO_4$ with spin rotation in the yz plane[20,34] which is also consistent with a dominating Fe^{2+} single-ion anisotropy.

The incommensurate magnetic state of $LiNiPO_4$, long range between 20.8 and 21.8 K and short range above, is the second outstanding feature in the $LiMPO_4$ family.[20] It points to the aforementioned competition between the NN and NNN exchange interactions within the yz plane which promotes incommensurability. The magnetic in-plane exchange is weakest along y direction[22] which may support that this is the orientation of the incommensurate propagation vector.

Here our data point to a relation between the incommensurate state and the AFM 180° domain structure. Plateletlike domains in $Li(Ni_{1-x}Fe_x)PO_4$ are observed in the samples where the long-range incommensurate order is observed, but in none of the other $LiMPO_4$ compounds. This strongly suggests that the domains are formed by breaking down the continuously varying incommensurate spin spiral "wave front" along y into discrete commensurately ordered AFM 180° domain platelets stacked along y. In $Li(Ni_{0.80}Fe_{0.20})PO_4$ the AFM domain structure is still not of the isotropic type seen in $LiCoPO_4$ or $LiFePO_4$. This may point to a residual tendency for an incommensurate spin arrangement, possibly of the short-range type that precedes the long-range incommensurate order.[20]

IV. SUMMARY AND CONCLUSIONS

In summary, the investigation of $Li(Ni_{1-x}Fe_x)PO_4$ single crystals by SHG reveals the competition between the respective magnetic order and domain structure of its end compounds, $LiNiPO_4$ and $LiFePO_4$. The magnetic structure of $Li(Ni_{0.94}Fe_{0.06})PO_4$ is the same as that of $LiNiPO_4$. As in $LiNiPO_4$ an isotropic domain topography not reflecting the magnetic anisotropy is found. We thus confirm earlier results obtained by neutron diffraction[34]: A substitution of 6% is too small for exerting fundamental changes in the magnetic structure. The magnetic properties of $Li(Ni_{0.80}Fe_{0.20})PO_4$ are found to be quite different from those of the two constituent materials. The competition between the Ni^{2+} and Fe^{2+} spin order leads to a low-symmetry magnetic structure which, according to the SHG data, has the point symmetry m. It implies that below 10 K the spins are rotated away from the principal axes in the (100) plane, including an angle of $40° \pm 3°$ with the y axis. The spin rotation decreases with increasing sample temperature until from 22.5 K and up to $T_N = 25.8$ K the spins point straight along the y axis as in $LiFePO_4$. The AFM domains in $Li(Ni_{0.80}Fe_{0.20})PO_4$ have a rodlike shape. The rods have a length of up to 1 mm and a width on the order of 10 μm. They are oriented in the (001) plane but with no preferred direction within this plane.

These observations reveal a range of information about the competition between different AFM 180° domain states in the $LiMPO_4$ system, which is a solid basis for understanding the mechanisms determining the formation of AFM 180° domain structures in general. In summary, we found the following:

(i) The observation that a Fe substitution of 6% is too small for exerting changes in the magnetic structure of $LiNiPO_4$ may be regarded as an unimposing result on first glance. However, it offers prospects for the investigation of the magnetic order in compounds whose electronic transitions are unfeasible for applying SHG. Here, low substitution with a low concentration of ions whose electronic transitions are in or close to the visible range would enable probing by SHG without yet affecting the magnetic structure. In particular, this can be applied to $LiMnPO_4$ where the lack of transitions in the visible range caused by the half-filled $3d$ shell prevented an investigation of the AFM domains so far. Such an investigation is highly desirable because with its different spin direction $LiMnPO_4$ is a key compound for understanding the relation between the transition-metal ions, their spin orientation, and the domain structure in the $LiMPO_4$ series.

(ii) The magnetic structure of the $Li(Ni_{1-x}Fe_x)PO_4$ system is revised. Note that the magnetic structure proposed here for $x = 20\%$ does not coincide with that of earlier neutron diffraction measurements[34] which favored the magnetic point symmetry $mm'm$ with spins aligned along the z axis up to the Néel temperature for which a value of 20.6 K was given. Most likely the contradiction was caused by the restricted set of diffraction reflections that focused on those dominated by the z component of the spin, like (0,1,0). The low value of the transition temperature would be in agreement with this assumption.

(iii) The investigation of the $Li(Ni_{1-x}Fe_x)PO_4$ domains at $x = 0.20$ reveals a variety of surprising aspects. An AFM structure with spins rotated in the (100) plane may be seen as a straightforward compromise between the z-oriented spins in $LiNiPO_4$ and the y-oriented spins in $LiFePO_4$. However, the distribution of the 180° domains, still a largely unexplored aspect of AFM materials, is by no means an obvious interpolation between the domain distributions found in the end compounds. Here, our work provides the basis for further exploration of this issue. In particular we observe a relation between the (short- and long-range) incommensurate AFM state in $Li(Ni_{1-x}Fe_x)PO_4$ and the formation of the subsequent 180° domains in the commensurate AFM phase.

(iv) The data point to an unusually large single-ion anisotropy of the Fe^{2+} ions which is consistent with other observations on the $LiMPO_4$ system. This information is important for developing a model for the single-ion anisotropy in the AFM $LiMPO_4$ family, which is currently in progress.[42]

ACKNOWLEDGMENTS

The authors thank the SFB 608 of the DFG for financial support. Research at Ames Laboratory is supported by the US Department of Energy, Office of Basic Energy Sciences, Division of Materials Sciences and Engineering under Contract No. DE-AC02-07CH11358.

*Corresponding author: manfred.fiebig@mat.ethz.ch

[1] Y. Tokura, Ed., *Colossal Magnetoresistive Oxides* (Gordon and Breach, London, 2000).
[2] P. W. Anderson, *The Theory of Superconductivity in the High-T_C Cuprate Superconductors* (Princeton University Press, Princeton, 1997).
[3] S. Loth, S. Baumann, C. P. Lutz, D. M. Eigler, and A. J. Heinrich, Science **335**, 196 (2012).
[4] A. Kimel, A. Kirilyuk, R. V. Pisarev, and T. Rasing, Nature (London) **429**, 850 (2004).
[5] N. P. Duong, T. Satoh, and M. Fiebig, Phys. Rev. Lett. **93**, 117402 (2004).
[6] R. Gómez-Abal, O. Ney, K. Satitkovitchai, and W. Hubner, Phys. Rev. Lett. **92**, 227402 (2004).
[7] W. Meiklejohn and C. Bean, Phys. Rev. **105**, 904 (1957).
[8] C. Tsang, R. Fontana, T. Lin, D. Heim, B. Speriosu, V. S. Gurney, and M. Williams, IEEE Trans. Magn. **30**, 3801 (1994).
[9] B. Dieny, J. Magn. Magn. Mater. **136** (1994).
[10] S. S. P. Parkin, K. P. Roche, M. G. Samant, P. M. Rice, R. B. Beyers, R. E. Scheuerlein, E. J. O'Sullivan, S. L. Brown, J. Bucchigano, D. W. Abraham *et al.*, J. Appl. Phys. **85**, 5828 (1999).
[11] R. E. Newnham, R. P. Santoro, and M. J. Redman, J. Phys. Chem. Solids **26**, 445 (1965).
[12] R. P. Santoro, D. J. Segal, and R. E. Newnham, J. Phys. Chem. Solids **27**, 1192 (1966).
[13] R. P. Santoro and R. E. Newnham, Acta Crystallogr. **22**, 344 (1966).
[14] H. Megaw, *Crystal Structures—A Working Approach* (Saunders, Philadelphia, 1973).
[15] R. Newnham and M. Redman, J. Am. Ceram. Soc. **48**, 547 (1965).
[16] I. Abrahams and K. Easson, Acta Crystallogr. Sect. C **49**, 925 (1993).
[17] F. Kubel, Z. Kristallogr. **209**, 755 (1994).
[18] J. M. Mays, Phys. Rev. **131**, 38 (1963).
[19] We use an optical instead of the crystallographic reference system with $x \sim a$, $y \sim b$, $z \sim c$.
[20] D. Vaknin, J. L. Zarestky, J.-P. Rivera, and H. Schmid, Phys. Rev. Lett. **92**, 207201 (2004).
[21] T. Jensen, N. Christensen, M. Kenzelmann, H. Ronnow, C. Niedermayer, N. Andersen, K. Lefmann, J. Schefer, M. v. Zimmermann, Y. Li *et al.*, Phys. Rev. B **79**, 092412 (2009).
[22] D. Vaknin, J. L. Zarestky, L. L. Miller, J.-P. Rivera, and H. Schmid, Phys. Rev. B **65**, 224414 (2002).
[23] J. Li, V. O. Garlea, J. L. Zarestky, and D. Vaknin, Phys. Rev. B **73**, 024410 (2006).
[24] N. Kharchenko, Y. Kharchenko, R. Szymczak, M. Baran, and H. Schmid, Low Temp. Phys. **27**, 895 (2001).
[25] N. Kharchenko, Y. Kharchenko, M. Baran, and R. Szymczak, Low Temp. Phys. **29**, 579 (2003).
[26] D. Arcon, A. Zorko, P. Cevc, R. Dominiko, M. Bele, J. Jamnik, Z. Jaglicic, and J. Glososcsky, J. Phys. Chem. Solids **65**, 1773 (2004).
[27] M. Mercier, J. Garayte, and E. Bertaut, CR Acad. Sci. B **264**, 979 (1967).
[28] M. Mercier, P. Bauer, and B. Fouilleux, CR Acad. Sci. B **267**, 1345 (1968).
[29] B. Van Aken, J.-P. Rivera, H. Schmidt, and M. Fiebig, Nature (London) **449**, 702 (2007).
[30] C. Ederer and N. A. Spaldin, Phys. Rev. B **76**, 214404 (2007).
[31] B. B. Van Aken, J. P. Rivera, H. Schmid, and M. Fiebig, Phys. Rev. Lett. **101**, 157202 (2008).
[32] A. S. Zimmermann, B. B. Van Aken, H. Schmid, J.-P. Rivera, J. Li, D. Vaknin, and M. Fiebig, Eur. Phys. J. B **71**, 355 (2009).
[33] A. S. Zimmerman, Ph.D. thesis, Universität Bonn, 2013.
[34] J. Li, T. B. S. Jensen, N. H. Andersen, J. L. Zarestky, R. W. McCallum, J.-H. Chung, J. W. Lynn, and D. Vaknin, Phys. Rev. B **79**, 174435 (2009).
[35] M. Schlenker and J. Baruchel, J. Appl. Phys. **49**, 1996 (1978).
[36] M. Fiebig, V. V. Pavlov, and R. V. Pisarev, J. Opt. Soc. Am. B **22**, 96 (2005).
[37] R. Birss, *Symmetry and Magnetism* (North-Holland, Amsterdam, 1966).
[38] M. Fiebig, D. Fröhlich, Th. Lottermoser, and K. Kohn, Appl. Phys. Lett. **77**, 4401 (2000).
[39] Th. Lottermoser, Ph.D. thesis, Universität Dortmund, Dortmund, 2002.
[40] M. Fiebig, Appl. Phys. B **74**, 749 (2002).
[41] D. Vaknin, J. L. Zarestky, J. E. Ostenson, B. C. Chakoumakos, A. Goñi, P. Pagliuso, T. Rojo, and G. E. Barberis, Phys. Rev. B **60**, 1100 (1999).
[42] E. Bousquet (private communication).
[43] R. M. Bozorth and V. Kramer, *Colloque International de Magnetisme de Grenoble* (CNRS Editions, Paris, 1959), p. 329.